Advanced Post-Processing Techniques of Molecular Dynamics Simulations in Studying Strong Anharmonic Thermodynamics of Solids

Tian Lan[1,2,*]

[1]*Department of Applied Physics and Materials Science,
California Institute of Technology, Pasadena, California 91125, USA*
[2]*Ginkgo LLC, Incline Village, Nevada, 89452, USA*
(Dated: October 20, 2015)

While the vibrational thermodynamics of materials with small anharmonicity at low temperatures has been understood well based on the harmonic phonons approximation; at high temperatures, this understanding must accommodate how phonons interact with other phonons or with other excitations. We shall see that the phonon-phonon interactions give rise to interesting coupling problems, and essentially modify the equilibrium and non-equilibrium properties of materials, e.g., thermal expansion, thermodynamic stability, heat capacity, optical properties, thermal transport and other nonlinear properties of materials. To date the anharmonic lattice dynamics is poorly understood despite its great importance, and most studies on lattice dynamics still rely on the harmonic or quasiharmonic models. With recent developement of computational models, the anharmonic information can be extracted from the atomic trajectories of molecular dynamics simulations. For example, the vibrational energy spectra, the effective potential energy surface and the phonon-phonon interaction channels can be derived from these trajectories which appear stochastic. These inter-dependent methods are adopted to successfully uncover the strong anharmonic phenomena while the traditional harmonic models fail dramatically, e.g., the negative thermal expansion of cuprite and the high temperature thermal stability of rutile.

I. INTRODUCTION

Today our understanding of the vibrational thermodynamics of materials at low temperatures is emerging nicely, based on the harmonic model in which phonons are independent. At high temperatures, however, this understanding is generally poor since it must accommodate how phonons interact with other phonons (so called anharmonic phonon-phonon interactions) or with electron or magnon excitations. These anharmonic processes and thermal excitations induce the frequency shifts and lifetime broadenings of the interacting quasi-particles, and contribute to most thermal properties at high temperatures.

These topics are rich and of great importance for the rational design and engineering of next-generation materials in energy based applications. For example, the anharmonic dynamics and other types of thermal excitations are the origin of most thermal energy transport processes, and therefore greatly influence the performance of these materials in applications of harvesting, storing and transporting energy. A reliable estimate of the anharmonic entropy is also crucial for synthesizing materials. For example, for metals and oxides, it seems that pure anharmonic contributions become large enough to affect phase stability at temperatures above half the melting temperature, which is the temperature range where materials are often processed or used. Anomaly in thermal expansion is another prominent example. Recently, the large negative thermal expansion (NTE) of ScF3 and Ag2O was found to have strong dependence with these high temperature vibrational dynamical properties.[1,2]

Modern inelastic scattering techniques with neutrons or photons are ideal for sorting these properties out.

Analysis of the experimental data can generate vibrational spectra of the materials, i.e., their phonon densities of states (DOS)and phonon or spin wave dispersions. We are developing the data reduction software to obtain the high quality data from inelastic neutron spectrometers. With accurate phonon DOS and dispersion curves we can obtain the vibrational entropies of different materials. The understanding of the underlying reasons for differences in DOS curves and entropies then relies on the development of the fundamental theories and the computational methods.

To date, most ab-initio methods for calculating materials structures and properties have been based on density functional (DFT) methods, and evaluating the internal energy, E, of materials at a temperature of zero Kelvin. For example, a harmonic or quasiharmonic model usually used to account for the vibrational thermodynamics at low temperatures and it is commonplace today to calculate harmonic phonons by methods based on DFT.[3] This can be adequate when the temperatures of service of the materials are low or when differences of chemical potential are much larger than kT. However, for most applications of materials in energy involving even modest temperature, this E alone is insufficient because the anharmonic vibrational dynamics and different types of thermal excitations become to play important roles and have significant thermodynamic effects at elevated temperatures.

Phonon-phonon interactions are responsible for pure anharmonicity that shortens phonon lifetimes and shifts phonon frequencies, especially at high temperatures. Anharmonicity competes with quasiharmonicity to alter the stability of phases at high temperatures, as has been shown, for example, with experiments and

frozen phonon calculations on bcc Zr[4] and the possible stabilization of bcc Fe-Ni alloys at conditions of the Earth's core.[5] For PbTe, ScF$_3$ and rutile TiO$_2$, there are recent reports of anharmonicity being so large that both the QHA and anharmonic perturbation theory fail dramatically.[1,6,7]

These cases are suitable for ab initio molecular dynamics (AIMD) simulations, which should be reliable when the electrons are near their ground states and the nuclear motions are classical. The big advantage of ab-initio MD is that it can account for all effects of harmonic, anharmonic and even some of the electron-phonon interactions. However, advanced post-processing methodologies are requied to extract concrete information from these simulations. In the few examples where comparisons have been made to ab-initio MD, agreement has been surprisingly good even for highly anharmonic materials. Today, by validating these calculated results with inelastic scattering experiments with facilities such as the Spallation Neutron Source for neutrons, we can obtain scientific details about phonon-phonon interactions, electron-phonon interactions and other excitations at elevated temperatures.

In this article, we discuss several MD-based computational techniques available just recently which proved useful for assessing the anharmonic vibrational thermodynamics of solids. The computational details are discussed in Section II, followed by a few examples shown in Section **??** and **??** that demonstrate how the applications of these inter-dependent methods can uncover interesting anharmonic properties of materials and their relationships with NTE, vibrational energy shift and phase stability.

II. COMPUTATIONAL METHODOLOGIES

A. Quasiharmonic Approximation

The quasiharmonic approximation (QHA) is based on how phonon frequencies change with volume. In the QHA, all shifts of phonon frequencies from their low temperature values are the result of thermal expansion alone.[3,8] Although the QHA accounts for some frequency shifts, the phonon modes are still assumed to be harmonic, non-interacting, and their energies depend only on the volume of the crystal.

In the quasiharmonic approximation, the vibrational free energy can be minimized as a function of volume,

$$F(V,T) = E_0 + \int\limits_{-\infty}^{+\infty} g(\omega)\left(\frac{\hbar\omega}{2} + k_B T \ln(1 - e^{-\hbar\omega/k_B T})\right) d\omega \,, \quad (1)$$

where E_0 is the energy calculated for the relaxed structure at $T = 0$ K. Thermodynamic properties are therefore derived from here.[3,8]

B. Molecular Dynamics Simulation

1. Molecular Dynamics Simulation and Fourier transformed velocity autocorrelation method

In non-harmonic potentials, phonon-phonon interactions are responsible for pure anharmonicity that shortens phonon lifetimes and shifts phonon frequencies. Anharmonicity competes with quasiharmonicity to alter the stability of phases at high temperatures. Velocity trajectories were extracted from the MD simulation at each temperature, and were then transformed to the corresponding vibrational energy and/or momentum domain.[2,7,9–12] Because the FTVAC method does not assume a form for the Hamiltonian, it is a robust tool for obtaining vibrational spectra from MD simulations, even with strong anharmonicity. The phonon DOS is given by

$$g(\omega) = \sum_{n,b} \int e^{-i\omega t} \langle \vec{v}_{n,b}(t)\, \vec{v}_{0,0}(0)\rangle\, dt \,, \quad (2)$$

where $\langle\,\rangle$ is an ensemble average, and $\vec{v}_{n,b}(t)$ is the velocity of the atom b in the unit cell n at time t. Further projection of the phonon modes onto each k point in the Brillouin zone was performed by computing the phonon power spectrum with the FTVAC method, with a resolution determined by the size of the supercell in the simulation.

2. Temperature-dependent effective potential method

In general, the cubic phonon anharmonicity contributes to both the phonon energy shift and the lifetime broadening, whereas the quartic anharmonicity contributes only to the phonon energy shift.[13,14] To distinguish the roles of cubic and quartic anharmonicity, the temperature-dependent effective potential (TDEP) method[7,15] was used. In the TDEP method, an effective model Hamiltonian is used to sample the potential energy surface, not at the equilibrium positions of atoms, but at the most probable positions for a given temperature in an MD simulation[15]

$$H = U_0 + \frac{1}{2}\sum_i m\mathbf{p}_i^2 + \frac{1}{2}\sum_{ij\alpha\beta} \phi_{ij}^{\alpha\beta} u_i^\alpha u_j^\beta \quad (3)$$

$$+ \frac{1}{3!}\sum_{ijk\alpha\beta\gamma} \psi_{ijk}^{\alpha\beta\gamma} u_i^\alpha u_j^\beta u_k^\gamma \,,$$

where ϕ_{ij} and ψ_{ijk} are second- and third-order force constants, $\mathbf{p}$ is momentum, and u_i^α is the Cartesian component α of the displacement of atom i. In the fitting, the "effective" harmonic force constants ϕ_{ij} are renormalized by the quartic anharmonicity. The cubic anharmonicity, however, is largely accounted for by the third-order force constants ψ_{ijk}, and can be understood in terms of

the third-order phonon self-energy that causes linewidth broadening.[13]

The resulting Hamiltonian was used to obtain the renormalized phonon dispersions (TDEP spectra) accounting for both the anharmonic shifts Δ, and broadenings Γ, of the mode $\vec{q}j$. These are derived from the real and imaginary parts of the cubic self-energies $\Sigma^{(3)}$, respectively.[13]

$$
\Delta(\vec{q}j;\Omega) = -\frac{18}{\hbar^2} \sum_{\vec{q}_1 j_1} \sum_{\vec{q}_2 j_2} \left|V(\vec{q}j;\vec{q}_1 j_1;\vec{q}_2 j_2)\right|^2 \Delta(\vec{q}_1 + \vec{q}_2 - \vec{q})
$$

$$
\times \wp \Big[\frac{n_1 + n_2 + 1}{\Omega + \omega_1 + \omega_2} - \frac{n_1 + n_2 + 1}{\Omega - \omega_1 - \omega_2}
$$

$$
+ \frac{n_1 - n_2}{\Omega - \omega_1 + \omega_2} - \frac{n_1 - n_2}{\Omega + \omega_1 - \omega_2} \Big] \tag{4}
$$

$$
\Gamma(\vec{q}j;\Omega) = \frac{18\pi}{\hbar^2} \sum_{\vec{q}_1 j_1} \sum_{\vec{q}_2 j_2} \left|V(\vec{q}j;\vec{q}_1 j_1;\vec{q}_2 j_2)\right|^2 \Delta(\vec{q}_1 + \vec{q}_2 - \vec{q})
$$

$$
\times \Big[(n_1 + n_2 + 1)\, \delta(\Omega - \omega_1 - \omega_2)
$$

$$
+ 2(n_1 - n_2)\, \delta(\Omega + \omega_1 - \omega_2) \Big], \tag{5}
$$

where Ω is the renormalized phonon frequency and $\wp$ denotes the Cauchy principal part. The $V(.)$'s are elements of the Fourier transformed third order force constants ψ_{ijk} obtained in the TDEP method. The $\Delta(\vec{q}_1 + \vec{q}_2 - \vec{q})$ ensures conservation of momentum.

C. Kinematics Functional of Phonon-Phonon Interactions

Anharmonicity tensors describe the coupling strengths for phonon-phonon interactions, but a prerequisite is that the phonons in these processes satisfy the kinematical conditions of conservation of energy and momentum as presented in Eq. 4 and 5. In the phonon-phonon interaction functional, an anharmonicity tensor element for an s-phonon process can be expressed as[16]

$$
V(j;\vec{q}_1 j_1;...;\vec{q}_{s-1} j_{s-1}) = \frac{1}{2s!} \left(\frac{\hbar}{2N}\right)^{\frac{s}{2}} N\, \Delta(\vec{q}_1 + \cdots + \vec{q}_{s-1})
$$

$$
\times [\omega_{j0}\omega_1 \cdots \omega_{s-1}]^{\frac{1}{2}} C(j;\vec{q}_1 j_1;...;\vec{q}_{s-1} j_{s-1}) \tag{6}
$$

where $\Delta(\vec{q}_1 + \cdots + \vec{q}_{s-1})$ enforces momentum conservation and the $C(.)$'s, elements of the s-phonon anharmonic tensor, are expected to be slowly-varying functions of their arguments.

If the anharmonicity tensor or its average does not vary significantly for different phonon processes, the coupling factor and the kinematic factor are approximately separable in Eq. 6. The separation of the anharmonic coupling and the kinematics has been used with success in many studies including our recent reports on rutile TiO_2 and SnO_2.[11,14] We consider the term $C(j;\vec{q}_1 j_1;...;\vec{q}_{s-1} j_{s-1})$ to be a constant of the Raman mode j, and use it as a fitting parameter. Although $C(j;\vec{q}_1 j_1;\vec{q}_2 j_2)$

and $C(j;j;\vec{q}_1 j_1;-\vec{q}_1 j_1)$ change with j_1 and j_2, an average over modes, $\langle C(.)\rangle = \sum_{1,2} C(j;\vec{q}_1 j_1;\vec{q}_2 j_2)/\sum_{1,2} 1$, is needed by the fitting, where 1, 2 under the summation symbol represent $\vec{q}_i j_i$. We define the cubic and quartic fitting parameters as

$$
C_j^{(3)} = \langle C(j;\vec{q}_1 j_1;\vec{q}_2 j_2)\rangle \tag{7a}
$$

$$
C_j^{(4)} = \langle C(j;j;\vec{q}_1 j_1;-\vec{q}_1 j_1)\rangle \tag{7b}
$$

To the leading order of cubic and quartic anharmonicity, the broadening of the Raman peaks is $2\Gamma^{(3)}(j;\Omega)$. The frequency shift of the Raman peaks is $\Delta^Q + \Delta^{(3)} + \Delta^{(3')} + \Delta^{(4)}$, where the quasiharmonic part is denoted by Δ^Q. These quantities can be written as functions of $D(\Omega, \omega_1, \omega_2)$ and $P(\Omega, \omega_1, \omega_2)$, weighted by average anharmonic coupling strengths[11,14]

$$
\Gamma^{(3)}(j;\Omega) = \frac{\pi\hbar}{64} \omega_{j0} \left|C_j^{(3)}\right|^2 \sum_{\vec{q}_1, j_1} \sum_{\vec{q}_2, j_2} \omega_1 \omega_2\, D(\Omega, \omega_1, \omega_2)
$$

$$
= \omega_{j0} \left|C_j^{(3)}\right|^2 D^\omega(\Omega) \tag{8a}
$$

$$
\Delta^{(3)}(j;\Omega) = -\frac{\hbar}{64} \omega_{j0} \left|C_j^{(3)}\right|^2 \sum_{\vec{q}_1, j_1} \sum_{\vec{q}_2, j_2} \omega_1 \omega_2\, P(\Omega, \omega_1, \omega_2)
$$

$$
= \omega_{j0} \left|C_j^{(3)}\right|^2 P^\omega(\Omega) \tag{8b}
$$

$$
\Delta^{(3')}(j) = -\frac{\hbar}{16N} \omega_{j0} \left|C_j^{(3)}\right|^2 \sum_{\vec{q}_2 j_2} \omega_{j_2}(\vec{q}_2) \left(n_{\vec{q}_2 j_2} + \tfrac{1}{2}\right) \tag{8c}
$$

$$
\Delta^{(4)}(j) = \frac{\hbar}{8N} \omega_{j0} C_j^{(4)} \sum_{\vec{q}_1 j_1} \omega_{j_1}(\vec{q}_1) \left(n_{\vec{q}_1 j_1} + \tfrac{1}{2}\right) \tag{8d}
$$

where $D^\omega(\Omega)$ and $P^\omega(\Omega)$ are functionals of $D(\Omega, \omega_1, \omega_2)$ and $P(\Omega, \omega_1, \omega_2)$ weighted by the kinematics of anharmonic phonon coupling. $D^\omega(\Omega)$ is the so-called two-phonon density of states (TDOS) spectra, which characterize the size of the phonon-phonon interaction channels. The $\Delta^{(3')}$ is an additional low-order cubic term that corresponds to instantaneous three-phonon processes.[13] It is nonzero for crystals having atoms without inversion symmetry, as in the case for the oxygen atom motions in the A_{1g} mode of rutile. It is much smaller than other contributions, however, owing to symmetry restrictions.

III. NEGATIVE THERMAL EXPANSION OF CUPRITE AG_2O AND ITS RELATIONSHIP WITH STRONG ANHARMONICITY

Silver oxide (Ag_2O) with the cuprite structure has attracted much interest after the discovery of its extraordinarily large negative thermal expansion (NTE),[17,18] which exceeds $-1\times10^{-5}\,K^{-1}$ and occurs over a wide range of temperature from 40 K to its decomposition temperature near 500 K.

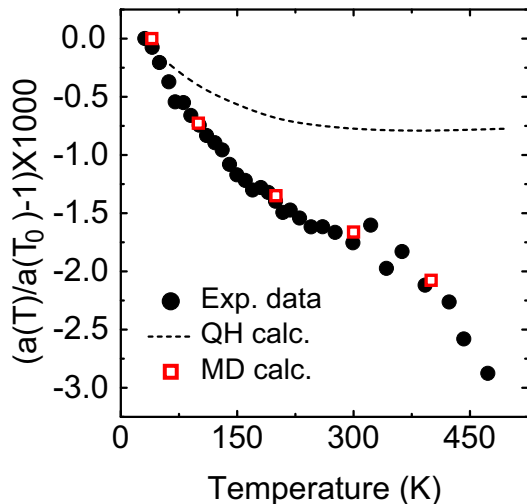A rigid-unit modes (RUMs) model of NTE considers tetrahedra of Ag_4O around each O atom that bend at

FIG. 1. Temperature dependence of lattice parameter from experimental data in Ref. [17], quasiharmonic calculations and MD calculations, expressed as the relative changes with respect to their 40 K values, i.e., $a(T)/a(40\,K) - 1$.

the Ag atoms linking the O atoms in adjacent tetrahedra. RUMs account for counteracting rotations of all such tetrahedra.[19,20] Locally, the O-Ag bond length does not contract, but bending of the O-Ag-O links pulls the O atoms together, leading to NTE. These RUMs tend to have low frequencies owing to the large mass of the unit, and hence are excited at low temperatures. This model correlateds the NTE with quasiharmonic approximation and should explain the main physics at low temperatures. However, as shown in Fig. 1, at temperatures above 250 K, there is a second part of the NTE behavior of cuprite Ag_2O that is apparently beyond the predictions of quasiharmonic theory.

A. Computational Methods and Results

First-principles calculations were performed with the generalized gradient approximation (GGA) of density functional theory (DFT), implemented in the VASP package.[21–23] Projector augmented wave pseudopotentials and a plane wave basis set with an energy cutoff of 500 eV were used in all calculations.

First-principles Born-Oppenheimer molecular dynamics simulations were performed for a $3 \times 3 \times 3$ supercell with temperature control by a Nosé thermostat. The relatively small simulation cell could be a cause for concern,[24] but convergence testing showed that the supercell in our study is large enough to accurately capture the phonon anharmonicity of Ag_2O. The simulated temperatures included 40, 100, 200, 300 and 400 K. For each temperature, the system was first equilibrated for 3 ps, then simulated for 18 ps with a time step of 3 fs. The system was fully relaxed at each temperature, with con-

vergence of the pressure within 1 kbar.

The phonon DOS curves calculated from first-principles MD simulations are shown in Fig. 2 with the experimental spectra for comparison. Excellent agreement is found between the simulated phonon DOS and the experimental data, and the calculated thermal broadenings and shifts are in good agreement, too.

Because of the large mass difference between Ag and O atoms, the O-dominated phonon modes are well separated from the Ag-dominated modes. Partial phonon DOS analysis showed that the Ag-dominated modes had similar energies, forming the peak of the phonon DOS below 20 meV (peak 1 in Fig. 2), whereas the O-dominated modes had energies above 40 meV (peaks 2 and 3).

This NTE above 250 K is predicted accurately by the ab-initio MD calculations, so it is evidently a consequence of phonon anharmonicity. The temperature-dependence of this NTE behavior follows the Planck occupancy factor for phonon modes above 50 meV, corresponding to the O-dominated band of optical frequencies. In the QHA these modes above 50 meV do not contribute to the NTE. These modes are highly anharmonic, however, as shown by their large broadenings and shifts.

B. Discussion

For cubic anharmonicity, as discussed, the two-phonon DOS (TDOS) is the spectral quantity parameterizing the number of phonon-phonon interaction channels available to a phonon. For Ag_2O with the cuprite structure, the peaks in the TDOS overlap well with the peaks in the phonon DOS. Most of the phonons therefore have many possible interactions with other phonons, which contributes to the large anharmonicity of Ag_2O with the cuprite structure, and small Q (short lifetimes). Although the Q values of most phonon modes in Ag_2O with the cuprite structure are small and similar, the origins of these lifetime broadenings are intrinsically different. For peak 2 of the phonon DOS, the anharmonicity is largely from the up-conversion processes: $O \mapsto O - Ag$, while for peak 3 it is from the down-conversion processes: $O \mapsto O + Ag$. The anharmonicity of peak 1 is more complicated. It involves both up-conversion and down-conversion processes of Ag-dominated modes. The TDOS also shows why the A_{2u} mode has a larger Q than other modes. Figure 3(b) shows that the A_{2u} mode lies in the trough of the TDOS where there are only a few phonon decay channels.

Owing to explicit anharmonicity from phonon-phonon interactions, the thermodynamic properties of Ag_2O with the cuprite structure cannot be understood as a sum of contributions from independent normal modes. The frequency of an anharmonic phonon depends on the level of excitation of other modes. At high temperatures, large vibrational amplitudes increase the anharmonic
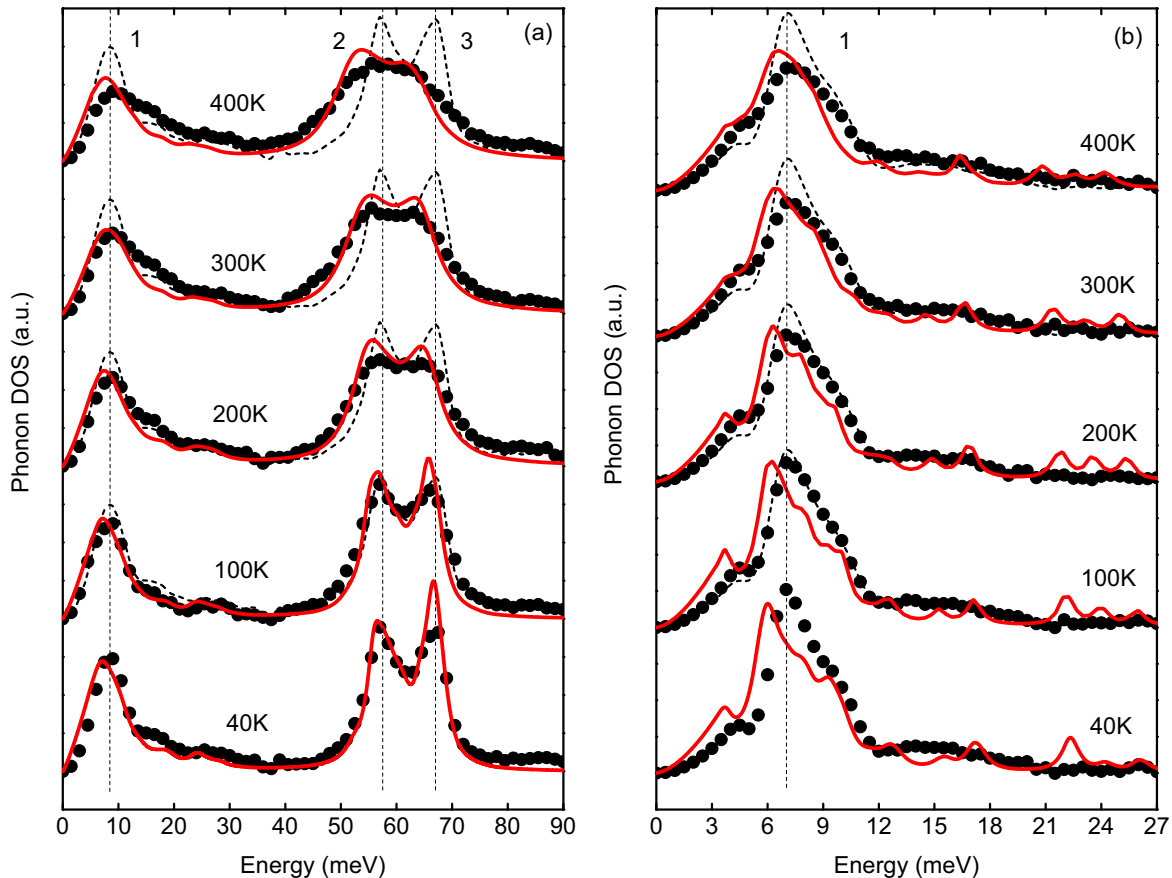
FIG. 2. Neutron weighted phonon DOS of Ag_2O with the cuprite structure from ARCS experimental data (black dots) and MD simulations (red curves) at temperatures from 40 to 400 K. The dashed spectrum corresponds to the 40 K experimental result, shifted vertically for comparison at each temperature. Vertical dashed lines are aligned to the major peak centers at 40 K from experiments, and are numbered at top. The incident energy was 100 meV for panel (a), and 30 meV for panel (b).

coupling of modes, and this increases the correlations between the motions of the Ag and O atoms, as shown by perturbation theory. Couplings in perturbation theory have phase coherence, so the coupling between Ag- and O-dominated modes at higher energies, as seen in the peak of the TDOS, causes correlations between the motions of Ag and O atoms. The ab-initio MD simulations show that anharmonic interactions allow the structure to become more compact with increasing vibrational amplitude. The mutual motions of the O and Ag atoms cause higher density as the atoms fill space more effectively. The large difference in atomic radii of Ag and O may contribute to this effect. Perhaps it also facilitates the irreversible changes in Ag_2O at temperatures above 500 K, but this requires further investigation. For cuprite Cu_2O, which has less of a difference in atomic radii, the thermal expansion is much less anomalous.

IV. THE QUARTIC PHONONS AND ITS STABILIZATION OF RUTILE PHASE OF TIO_2

Although the rutile structure of TiO_2 is stable at high temperatures, the conventional quasiharmonic approximation predicts that several acoustic phonons decrease anomalously to zero frequency with thermal expansion, incorrectly predicting a structural collapse at temperatures well below 1000 K.[25,26] Inelastic neutron scattering was used to measure the temperature dependence of the phonon density of states (DOS) of rutile TiO_2 from 300 to 1373 K. Surprisingly, these anomalous acoustic phonons were found to increase in frequency with temperature.[7]

A. Computational Methods and Results

First-principles calculations using the local density approximation (LDA) of density functional theory (DFT) were performed with the VASP package.[21,23] Projector augmented wave pseudopotentials and a plane wave basis set with an energy cutoff of 500 eV were used in
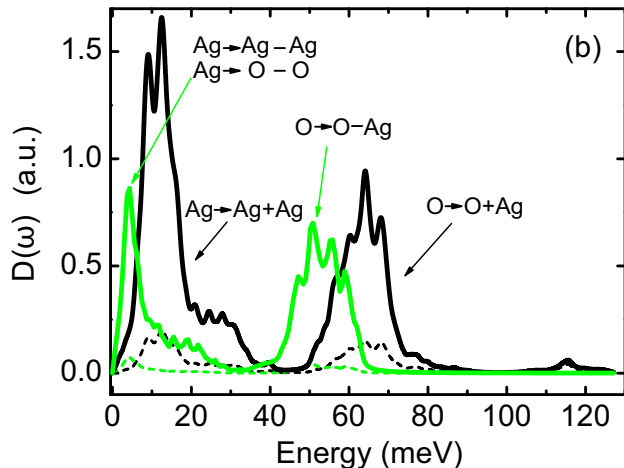
FIG. 3. The TDOS spectra, $D(\omega)$, at 40 K (dashed) and 400 K (solid). The down-conversion and up-conversion contributions are presented separately as black and green curves, respectively.

all calculations. Previous work showed that for best accuracy, the Ti pseudopotential should treat the semicore $3s$ and $3p$ states as valence,[25–27] and we took this approach with a similar LDA functional. Our calculated elastic properties, lattice dynamics, and dielectric properties derived from the optimized structure for 0 K, were in good agreement with results from experiment and from previous DFT calculations.

First-principles Born-Oppenheimer AIMD simulations for a $2 \times 2 \times 4$ supercell and a $2 \times 2 \times 1$ k-point sampling were performed to thermally excite phonons to the target temperatures of 300 and 1373 K. For each temperature, the system was first equilibrated for 3 ps as an NVT ensemble with temperature control by a Nosé thermostat, then simulated as an NVE ensemble for 20 ps with time steps of 1 fs. Good relaxations with residual pressures below 0.5 GPa were achieved in each calculation that accounted for thermal expansion.

Figure 4 shows the vibrational energies of the TA branch, calculated by the FTVAC method with AIMD trajectories. From 300 to 1373 K, the TA branch increases in energy by an average of about 2.1 meV. Especially for this TA branch, Fig. 4(b) shows an enormous discrepancy of phonon energies between the MD calculation and the QHA (orange dashed line) at 1373 K. The unstable phonon modes predicted by the QHA are fully stable in the AIMD simulations at high temperatures, however.

Using the same MD trajectories as for the FTVAC method, the calculated TDEP dispersions agree well with the FTVAC results as shown in Fig. 4(a)(b). The cubic anharmonicity of rutile TiO_2 is strong for phonons at energies above 25 meV,[11] causing broadening of the phonon DOS and the dispersions. Nevertheless, at 1373 K the TA modes below 20 meV have only small linewidth broadenings. Furthermore, they are close in

energy to those calculated if all ψ_{ijk} are set to zero in Eq. 3, showing the dominance of quartic anharmonicity and the small cubic anharmonicity of the TA modes.

For more details about the anomalous anharmonicity of the TA modes, the frozen phonon method was used to calculate potential energy surfaces for specific phonons, as in Fig. 4(c). At 300 K the potential energy of the TA mode at the R-point is nearly quadratic, with a small quartic part. With the lattice expansion characteristic of 1373 K, the potential energy curve transforms to being nearly quartic. In fact, for all modes in the TA branch that were evaluated by the frozen phonon method, the potential energy surface develops a quartic form with lattice expansion For a quantum quartic oscillator, the vibrational frequency stiffens with temperature owing to the increasing spread between the energy levels.[1,28] We assessed a high temperature behavior by assigning Boltzmann factors to the different oscillator levels derived from frozen phonon potentials, giving the energies of the quartic TA modes at 1373 K. As shown in Fig. 4(b), they are reasonably close to the FTVAC and TDEP results.

B. Discussion

The patterns of atom displacements in the anomalous modes at Γ, R, and along Z-Γ, Γ-M, and M-A were identified, and those for the R point in Fig. 5(a) are typical. In these anomalous modes, the O atoms were approximately stationary, and each O atom has a Ti neighbor that moves towards it and another Ti neighbor that moves away from it by approximately the same amount. These modes have "ring" patterns in which displacements of Ti atoms rotate a structural unit, and all the O atoms see approximately the same change in their Ti neighborhood. In the positive and negative displacements of these modes, the O atoms show an accumulation of charge in the Ti–O bond of shorter distance and a depletion in the bond of longer distance, as indicated by a much higher value of the electron localization function (ELF)[29] for the short bond shown in Fig. 5(b).

We calculated the "bond-weighted" electron DOS by partitioning the band structure energy into bonding and no-bonding contributions and obtaining the crystal orbital Hamilton population (COHP) spectrum[30] of rutile with different lattice parameters in a $2 \times 2 \times 4$ supercell. Figure 5(c) shows the COHP spectrum of the bonds formed by the Ti $3d$ and O $2p$ orbitals between 5.5 and 3.5 eV below the Fermi energy. With lattice expansion (of 1% or 2%), these bonding states become less favorable, and their COHP spread narrows. Also shown in color in Fig. 5(b) is the COHP with a frozen phonon mode at the R-point having 0.14 Å displacements of Ti atoms. On the scale of thermal energies, the broadening effect from the phonon changes considerably with lattice expansion.

With an increase in lattice parameter, the longer Ti–O bond makes a smaller contribution to the interatomic
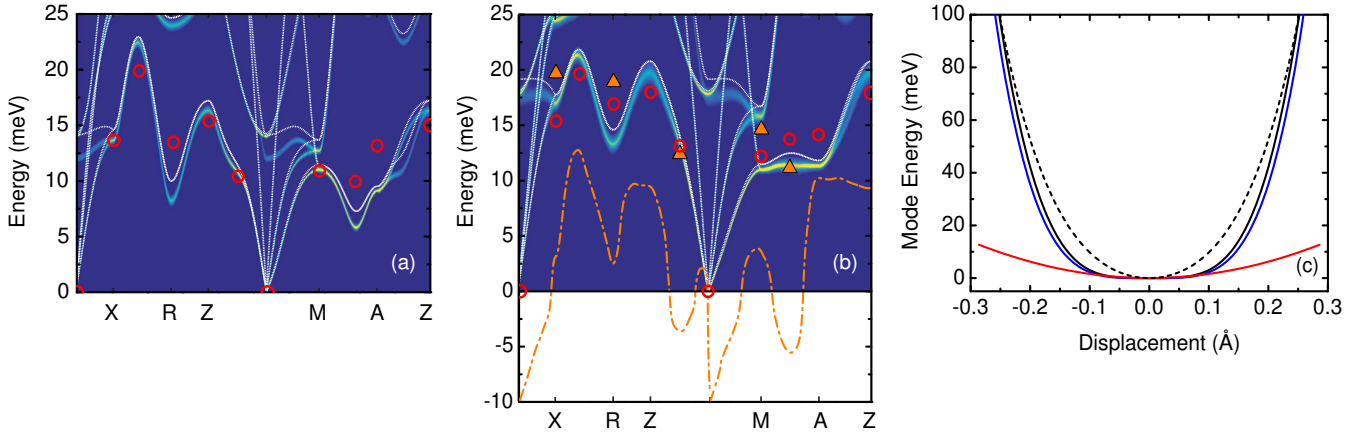
FIG. 4. Diffuse curves are TDEP phonon dispersions below 25 meV at (a) 300 K, and (b) 1373 K, compared with the results from the FTVAC method (red circles). The white curves are phonon dispersions for the quasiharmonicity plus quartic anharmonicity calculated with all ψ_{ijk} set to zero in Eq. 3. In (b), the dispersions are compared to the quasiharmonic dispersions (orange dashed curve) and the single quartic oscillator model (orange triangles). (c) Frozen phonon potential (black) of TA mode at R point with $q = (0.5, 0, 0.5)$ at 1373 K, showing the harmonic component (red) and quartic component (blue). The low temperature potential surface is also shown (dashed black).
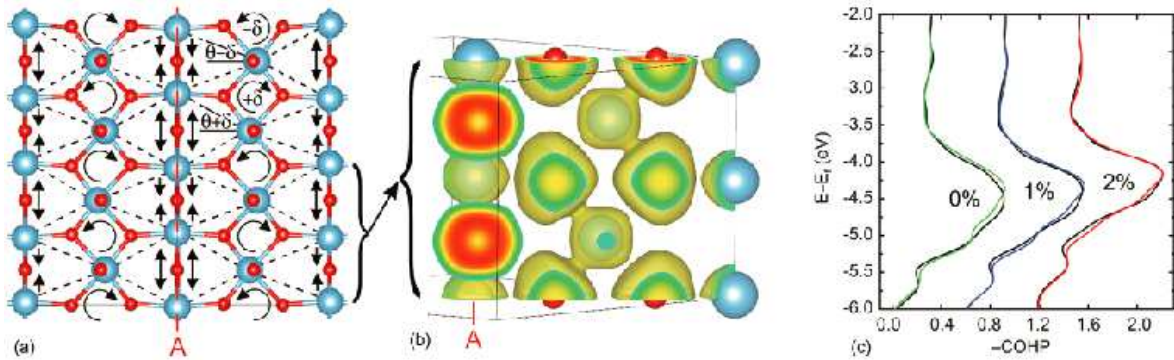

FIG. 5. (a) Displacements of atoms for the TA mode at the R-point in the (1-10) plane. Light blue spheres are Ti atoms, and O atoms are red. Arrows depict distortions of the structural units (dashed rhombuses). The rotational movements of structures, or the "ring" patterns, are indicated with circled arrows. (b) ELF isosurface of a "ring" shown in (a) with the value of 0.3. The ELF increase is apparent in the bond of shorter distance owing to the ring displacement. The ELF is the probability measure of finding an electron at a location given the existence of neighbouring electrons. It ranges from 0 (no electron) to 1 (perfect localization). (c) COHP analysis of Ti–O bonds for equilibrium lattice parameter at $T=0$ K (0%), and for linear expansions of 1% and 2%. Shown in color are –COHP results for the same structures with the phonon of panel (a) having 0.14 Å normal displacements of Ti atoms. Curves for 1% and 2% expansion are offset by 0.6 and 1.2.

force during its vibrational cycle. The shorter Ti–O bond gives a stronger hybridization of Ti $3d$ – O $2p$ orbitals as the Ti atom moves closer to the O atom. The hybridization serves to offset the energy of short-range repulsion. With lattice expansion, the short-range repulsion is weaker, and hybridization favors electrons between the shorter Ti–O pairs in the phonon displacement pattern. The "ring" patterns of the phonons play an important role in increasing the degree of hybridization as they complete the electron back-donation cycles from the O to the Ti atoms. For example, a 3% decrease of Bader effective charge (+2.22 at equilibrium) was found

for the Ti atoms with 0.14 Å displacments in the "ring" patterns, which is comparable to the charge decrease of the Ti atoms during the ferroelectric transition of rutile.[27] However, if Ti atoms along the direction "A" were locked down at their equilibrium positions so the ring motion is broken, the resulting decrease of the effective charge dropped by 50% to 70% in the "ring" patterns. The potential was found to rise, and was largely quadratic even at 1% or 2% expansion.

A macroscopic elastic response to this phonon can also be identified with the assistance of Fig. 5(a). In equilibrium, the apex angles of the rhombuses are all equal, but with the rotation by δ, the vertical stretching of rhom-

buses along the line A is $2a\sin(\theta+\delta)$, and the contraction is $2a\sin(\theta-\delta)$, where θ is the semi-angle of the rhombus. For small δ, a Taylor expansion gives a net vertical (or horizontal) distortion of $-2a\delta^2\sin\theta$ (or $-2a\delta^2\cos\theta$). The distortions are proportional to δ^2, while the atom displacements in this TA mode are proportional to δ. A strain energy that goes as the square of this distortion is consistent with a quartic potential.

The hybridization in the Ti–O bond is very sensitive to interatomic distance, much as has been noticed in the ferroelectric distortion of $BaTiO_3$.[31] For rutile TiO_2, however, the hybridization follows the atom displacements in thermal phonons (instead of a displacive phase transition), and this "phonon-tracked hybridization" changes with lattice parameter. It provides a source of extreme phonon anharmonicity, but also provides thermodynamic stability for rutile TiO_2. It may occur in other transition metal oxides that show unusual changes of properties with lattice parameter or with structure, and such materials may be tunable with composition or pressure to control this effect. Besides altering thermodynamic phase stability, properties such as ferroelectricity and thermal transport will be affected directly.

V. CONCLUSIONS

The study of phonon anharmonicity and phonon-phonon interaction is a difficult but exciting field. It is difficult because we must consider how phonons interact with other phonons or with other excitations, which is an example of notorious manybody interaction problem. In comparison, our understanding today about the vibrational thermodynamics of materials at low temperatures is broad and deep because it is based on the harmonic model in which phonons are independent, avoiding issues of anharmonic lattice dynamics. However, the failure of the harmonic theory also mostly arises from the assumption of independent phonons, which becomes increasingly inaccurate at high temperatures.

With the development of molecular dynamics simulations and the progress of the anharmonic phonon theories and computational methodologies based upon it, we are now in a good position to study the relation between the phonon anharmonicity and many important thermodynamic properties of materials especially at high temperatures. For example, advanced computational methods being discussed in this paper provided the microscopic perspective of phonon anharmonicty and its relationship with the thermodynamic phase stability of rutile TiO_2 and anomaly thermal expansion of cuprite Ag_2O.

* tian@ginkgo-llc.com

[1] C. W. Li, X. Tang, J. A. Muñoz, J. B. Keith, S. J. Tracy, D. L. Abernathy, and B. Fultz, Phys. Rev. Lett. **107**, 195504 (2011).

[2] T. Lan, C. W. Li, J. L. Niedziela, H. Smith, D. L. Abernathy, G. R. Rossman, and B. Fultz, Phys. Rev. B **89**, 054306 (2014).

[3] B. Fultz, Prog. Mater. Sci. **55**, 247 (2010).

[4] Y. Ye, Y. Chen, K. Ho, B. N. Harmon, and P. Lindgard, Phys. Rev. Lett. **58**, 1769 (1987).

[5] L. Dubrovinsky, N. Dubrovinskaia, O. Narygina, I. Kantor, A. Kuznetzov, V. B. Prakapenka, L. Vitos, B. Johansson, A. S. Mikhaylushkin, S. I. Simak, and I. A. Abrikosov, Science **316**, 1880 (2007).

[6] O. Delaire, J. Ma, K. Marty, A. F. May, M. A. McGuire, M.-H. Du, D. J. Singh, A. Podlersnyak, G. Ehlers, M. D. Lumsden, and B. C. Sales, Nature Materials **10**, 614 (2011).

[7] T. Lan, C. W. Li, O. Hellman, D. Kim, J. A. Muñoz, H. Smith, D. L. Abernathy, and B. Fultz, Phys. Rev. B **92**, 054304 (2015).

[8] C. W. Li, H. L. Smith, T. Lan, J. L. Niedziela, J. A. Muñoz, J. B. Keith, L. Mauger, D. L. Abernathy, and B. Fultz, Phys. Rev. B **91**, 144302 (2015).

[9] N. de Koker, Phys. Rev. Lett. **103**, 125902 (2009).

[10] J. A. Thomas, J. E. Turney, R. M. Iutzi, C. H. Amon, and A. J. H. McGaughey, Phys. Rev. B **81**, 081411 (2010).

[11] T. Lan, X. Tang, and B. Fultz, Phys. Rev. B **85**, 094305 (2012).

[12] T. Lan, *Studies of phonon anharmonicity in solids*, Ph.D. thesis, California Institute of Technology (2014).

[13] A. A. Maradudin and A. E. Fein, Phys. Rev. **128**, 2589 (1962).

[14] T. Lan, C. W. Li, and B. Fultz, Phys. Rev. B **86**, 134302 (2012).

[15] O. Hellman and I. A. Abrikosov, Phys. Rev. B **88**, 144301 (2013).

[16] I. P. Ipatova, A. A. Maradudin, and R. F. Wallis, Phys. Rev. **155**, 882 (1967).

[17] W. Tiano, M. Dapiaggi, and G. Artioli, J. Appl. Crystallogr. **36**, 1461 (2003).

[18] B. J. Kennedy, Y. Kubota, and K. Kato, Solid State Commun. **136**, 177 (2005).

[19] A. K. A. Pryde, K. D. Hammonds, M. T. Dove, V. Heine, J. D. Gale, and M. C. Warren, J. Phys.-Condens. Matter **8**, 10973 (1996).

[20] V. Heine, P. R. L. Welche, and M. T. Dove, J. Am. Ceram. Soc. **82**, 1793 (1999).

[21] G. Kresse and D. Joubert, Phys. Rev. B **59**, 1758 (1999).

[22] G. Kresse and J. J. Hafner, Phys. Rev. B **47**, 558 (1993).

[23] G. Kresse and J. Furthmüller, Phys. Rev. B **54**, 11169 (1996).

[24] D. P. Sellan, E. S. Landry, J. E. Turney, A. J. H. McGaughey, and C. H. Amon, Phys. Rev. B **81**, 214305 (2010).

[25] P. D. Mitev, K. Hermansson, B. Montanari, and K. Refson, Phys. Rev. B **81**, 134303 (2010).

[26] K. Refson, B. Montanari, P. D. Mitev, K. Hermansson, and N. M. Harrison, Phys. Rev. B **88**, 136101 (2013).

[27] B. Montanari and N. M. Harrison, J. Phys.: Condens. Matter **16**, 273 (2004).

[28] P. Dorey and R. Tateo, J. Phys. A **32**, L419 (1999).

[29] B. Silvi and A. Savin, Nature **371**, 683 (1994).

[30] S. Maintz, V. L. Deringer, A. L. Tchougreeff, and R. Dronskowski, J. Comput. Chem. **34**, 2557 (2013).

[31] R. E. Cohen, Nature **358**, 136 (1992).